The Report committee for Khurram Usman Mazher
certifies that this is the approved version of the following report:

Automotive Radar Using IEEE 802.11p Signals

APPROVED BY

SUPERVISING COMMITTEE:

Robert W. Heath Jr., Supervisor

Nuria Gonzalez-Prelcic

Automotive Radar Using IEEE 802.11p Signals

by

Khurram Usman Mazher

REPORT

Presented to the Faculty of the Graduate School of

The University of Texas at Austin

in Partial Fulfillment

of the Requirements

for the Degree of

MASTER OF SCIENCE IN ENGINEERING

THE UNIVERSITY OF TEXAS AT AUSTIN

May 2019

Dedicated to HM

Acknowledgments

I gratefully acknowledge the support of Toyota InfoTechnology Centre, U.S.A., Inc. for funding this work.

I also acknowledge the gracious support and *tolerance* of my family, HM, friends, Piper, Winnie, Pixie, colleagues, teachers and advisors, both current and previous. I also thank Dr. Nuria Gonzalez-Prelcic for agreeing to be my reader for this report. Last but not the least, I would like to thank Dr. Amine Mezghani for his valuable insights, ideas, support and all the time he has put in with me.

Automotive Radar Using IEEE 802.11p Signals

Khurram Usman Mazher, M.S.E.
The University of Texas at Austin, 2019

Supervisor: Robert W. Heath Jr.

Autonomous vehicles have led to a surge in research on automotive radar both in academia and industry during the last few years. In this report, we develop a framework for using the dedicated short range communication (DSRC) waveform for the purposes of automotive radar. Our approach operates on the frequency domain channel estimates generated by the OFDM physical layer used in DSRC. We consider a two path channel model, with the first cluster corresponding to direct signal interference and the second cluster corresponding to the signal reflected from the target. The target ranging, direction of arrival and velocity information is encoded in the parameters of the reflected path. We estimate the parameters of the direct and reflected path using a variant of least squares matching pursuit algorithm by exploiting their relative power difference. The performance of the algorithm is evaluated through numerical simulations assuming low power omnidirectional 5 dBi antennas, Swerling type 0 and type 3 target models, 10 MHz transmission bandwidth and different analog-to-digital quantization resolutions. Simulations results show sub-meter accuracy in location estimation for a significant

range of target distances. The results are also compared with the Cramer-Rao lower bound which is a theoretical performance benchmark.

Table of Contents

List of Tables

List of Figures

Chapter 1

Introduction

The National Transportation Safety Board has recommended frontal collision detection systems to be installed as standard equipment on all new vehicles [1]. Radar is one of the primary sensors required for this operation. Vehicular radars are usually implemented in the millimeter wave (mmWave) band, use large bandwidth, specialized circuitry, and antenna arrays[2]. DSRC standard is the primary candidate for vehicle-to-vehicle (V2V) communication. An alternative means of collision avoidance is to make use of the DSRC standard for V2V communication. In this system, vehicles broadcast their position and other information, which can be used for forward collision warning and other applications. Unfortunately, DSRC is only useful in this way when the other vehicle also supports DSRC. As a result, it does not replace the need for radar to sense unconnected vehicles.

MmWave radars require antenna arrays and special circuitry for adequate operation, thus leading to increased costs. The mmWave circuitry and antennas are packaged as a single entity to avoid cable losses at high frequency. This makes the radar unit more susceptible to damage upon collisions [2], as they are usually installed in the bumpers. This report presents a joint radar-

communication system based on DSRC that will be a cheaper alternative to traditional vehicular radars, use a much smaller BW, help take advantage of the V2V systems being adopted by automobile manufacturers at a fast pace and provide additional benefits in terms of packaging, installation and security.

In this report, we propose a joint radar-communication system based on the DSRC hardware and signal waveform. DSRC is based on the IEEE 802.11p standard. The IEEE 802.11p physical layer (PHY) uses the orthogonal frequency division multiplexing (OFDM) waveform and will commonly employ a 10 MHz bandwidth [3]. The proposed range, direction of arrival (DoA) and velocity estimation algorithms operate on the frequency domain channel estimates provided by the IEEE 802.11p based DSRC receiver. They explicitly take into account the presence of the strong direct path interference resulting from the omnidirectional antennas (intended for communication), use the direct path as a timing reference, and thus do not require access to the DSRC system clock. We assume a setup with one TX antenna and two RX antennas placed on the vehicle roof. Our algorithm uses the order recursive least squares matching pursuit (LS-MP) algorithm described in [4] to find good estimates of the parameters of the direct and reflected path. The algorithm first estimates the parameters of the direct path by exploiting the strong difference in power between the two paths. Subsequently the parameters of the reflected path which encode the target range, DoA and velocity information are estimated by jointly minimizing the error over the direct and reflected path parameters. Simulation results show that the LS-MP based algorithm gives

target location estimates with sub-meter accuracy for targets up to distance of 45m and achieves the Cramer-Rao lower bound (CRLB) for medium to larger target distances.

Joint radar-communication systems and OFDM based radars have been investigated in [5–12]. Range estimation based on the inverse discrete Fourier transform (IDFT) of the frequency domain channel estimate was proposed in [5, 6]. A similar method based on the IDFT of one particular sub-carrier across multiple OFDM symbols was investigated in [7] for velocity estimation of the target. Time of arrival (ToA) estimation based on the phase of autocorrelation of training sequence has been proposed in [8]. Similarly [9] proposed a method for ToA estimation based on the MUltiple SIgnal Classification (MUSIC) algorithm. Range and velocity estimation using the cross-correlation function and a clutter cancellation algorithm were investigated in [10]. These papers assume access to the timing clock to provide them with accurate information about the start of transmission and reception. Unlike a traditional radar, DSRC hardware does not necessarily expose access to the system timing clock in the baseband signal processing. Without a timing reference, the reception of signals at a time instant other than the exact discrete sampling bins and any timing synchronization errors in the IEEE 802.11p receiver can change the phase information which encodes the distance to the target. Another common aspect of all these papers is that they fail to point out that the reflections from the target will be masked by a very strong direct path because of the omni-directional gain pattern (for communication purposes) of the antennas in case

of co-located transmit (TX) and receive (RX) antennas (maximum separation of vehicle width). This direct path can not be avoided unless full duplex cancellation is exploited [13]. The direct path was explicitly modeled and used to make a simplification in [11, 12]. The multi-dimensional brute force search used to estimate the channel parameters in [11, 12] is not extendable to a multiple target scenario, does not provide DoA information, and assumes high gain directional antennas. The algorithm proposed in this report is extendible to multiple target scenarios, provides DoA estimates and does not require/assume high gain directional antennas. The direct path, which acts as the timing reference for our algorithms, needs to be cancelled out after synchronization for target detection. Least squares based method for clutter cancellation [14] and methods based on adaptive filters [15] are not adequate because the residual of the direct path after cancellation still overpowers the target signal. The strong direct path also rules out methods used in traditional array processing for DoA estimation such as [16], [17] where a far field signal model is assumed under which the signals impinging on the antenna elements differ only in phase.

Note: A part of this work was published in IEEE WCNC 2018 [18].

Notation: Vectors are denoted by boldface lowercase letters $\mathbf{v}$, matrices are denoted by boldface capital letters $\mathbf{V}$ and scalar values by v, V. $\angle v$ denotes the phase of v. $\mathbf{v}^*$ and v^* denote the conjugate transpose and conjugate of vectors and scalars. $||\mathbf{v}||_2^2$ denotes the l_2 norm of $\mathbf{v}$. $|\mathbf{v}|$ denotes the number of elements in vector $\mathbf{v}$.

Chapter 2

System and Channel Model

In this chapter, the system model and the radar channel model are described in detail.

2.1 System Model

Fig. 2.1 shows the V2V system considered in this report. The top half of Fig. 2.1 illustrates the case when DSRC is being used as a communication modality. When operating in communication mode, the transmission and reception take place on separate vehicles. The bottom half of Fig. 2.1 depicts the case when the DSRC system is being operated in Radar mode. This setup is similar to that of a mono-static radar and is used for single target detection in this report.

The omnidirectional nature of the antennas results in a two path channel model as shown in Fig. 2.1. This is a common channel model in mono-static OFDM radars [5, 10–12] and can be extended to multiple targets by incorporating their reflected paths [6, 7]. The TX and RX antennas are separated by the vehicle width = 1.5m. The two RX antennas are separated by a distance $d = \frac{\lambda}{2}$ where λ is the wavelength corresponding to the carrier frequency f_c.

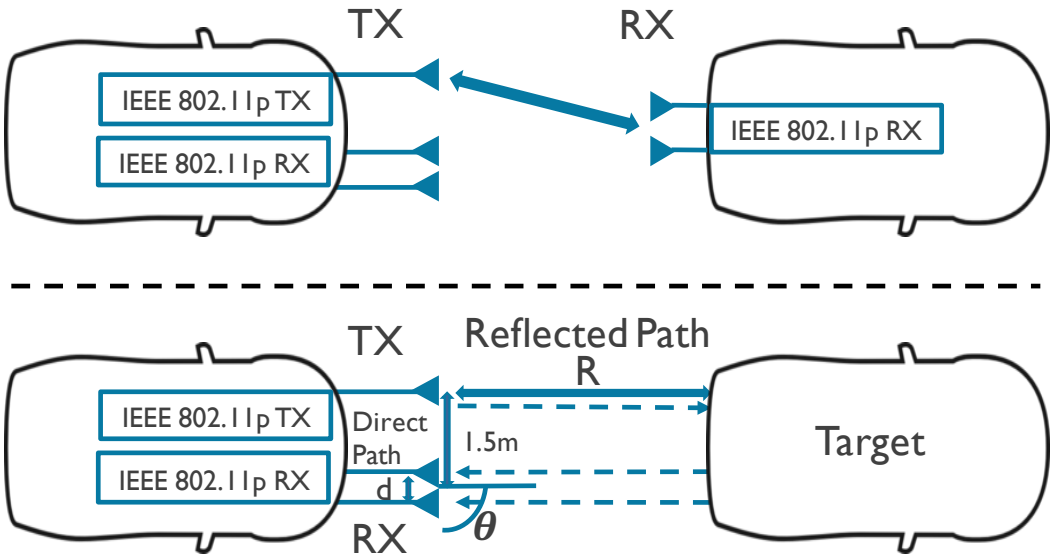

Figure 2.1: Single target channel model. The top half illustrates the use of DSRC as a communication tool. The bottom half depicts DSRC operation in radar mode.

The delay from the TX antenna to the first and second RX antenna is denoted by τ_{d_1} and τ_{d_2}. The round trip time from the TX antenna to the RX antennas given by τ is related to the distance R from the target vehicle by $\frac{2R}{c}$ where c is the speed of light. The combined affect of antenna gains and path loss along the direct path from the TX antenna to the two RX antennas is represented by α_{d_1} and α_{d_1}. Similarly, α is the end to end gain along the reflected path and additionally includes the effect of reflection cross-section (RCS) area of the target vehicle. We consider two types of target models in this work: the Swerling type 0 and the Swerling type 3 [19]. Swerling type 0 targets are fixed amplitude targets characterized by their RCS area ζ whereas Swerling

type 3 targets are modeled by a fixed amplitude part corresponding to the line of sight (LOS) path and a Rayleigh part corresponding to a rich scattering environment which changes independently from scan to scan. The phase of the Rayleigh part of the target is independently distributed on $(-\pi, \pi]$. The amount of power in the Rayleigh part given by γ, is modeled as a percentage of the power in the LOS path ζ.

2.2 Channel Model

Under the narrowband assumption, the reflected signal at the second RX antenna contains an additional phase difference $\phi = \frac{2\pi \mathrm{d} \cos\theta}{\lambda}$ compared to the first RX antenna, where θ is the angle measured from the line parallel to the line joining the antennas. With all the parameters defined, the continuous time channel from the TX antenna to the first and second RX antenna can be written as

$$\begin{aligned} h_1(t) &= \alpha_{\mathrm{d}_1}\delta(t-\tau_{\mathrm{d}_1}) + \alpha\delta(t-\tau), \\ h_2(t) &= \alpha_{\mathrm{d}_2}\delta(t-\tau_{\mathrm{d}_2}) + \alpha e^{j\phi}\delta(t-\tau). \end{aligned} \tag{2.1}$$

The direct path gain of both RX antennas is modeled by separate parameters, α_{d_1} and α_{d_1}, which emphasizes the fact that the self interference can not be simply modeled as another source impinging on the RX antennas with the same power. The direct signal interference is so strong compared to the reflected path (40dB $-$ 80dB using the parameters in Chapter 5) that any residues resulting from modeling it using a common parameter α_{d} at both RX antennas will have large magnitudes and adversely affect the parameter

estimation. This will also hold true when estimating the direct path parameters for cancellation. Further the direct path impinges in the endfire direction making it more difficult to cancel.

The radar estimation problem can be formulated as a sinusoid parameter estimation problem in terms of the frequency domain spectrum of the channel impulse response in (2.1). The baseband discrete-time frequency domain channel estimates of the channel impulse response in (2.1) after being filtered to the bandwidth occupied by the transmitted signal and sampled at the Nyquist rate f_s are given by

$$\begin{aligned} H_1(e^{j2\pi f}) &= \alpha_{\mathrm{d}_1} e^{-j2\pi f_c \tau_{\mathrm{d}_1}} e^{-j2\pi f \tau_{\mathrm{d}_1} f_s} + \alpha e^{-j2\pi f_c \tau} e^{-j2\pi f \tau f_s}, \\ H_2(e^{j2\pi f}) &= \alpha_{\mathrm{d}_2} e^{-j2\pi f_c \tau_{\mathrm{d}_2}} e^{-j2\pi f \tau_{\mathrm{d}_2} f_s} + \alpha e^{-j(2\pi f_c \tau - \phi)} e^{-j2\pi f \tau f_s}. \end{aligned} \tag{2.2}$$

The frequency domain channel estimates calculated by the IEEE 802.11p receiver are equally spaced samples of the spectrum in (2.2) estimated using the long training preamble sequence. Let N denote the number of sub-carriers of the transmitted waveform. The equally spaced samples of frequency spectrum can be written as $n\Delta f$ where $\Delta f = \frac{B}{N} = \frac{f_s}{N}$, $n \in \{\frac{-N}{2}, \ldots 0, \ldots \frac{N}{2} - 1\}$ and B is the bandwidth of the transmitted waveform. In the case of IEEE 802.11p $N = 64$. Of these 64 only $N_c = 52$ sub-carriers are used for transmission, with the remaining 12 acting as guard bands and DC null. Of these 52 sub-carriers $N_p = 4$ sub-carriers are used as pilots to estimate any residual phase offsets from one OFDM symbol to the next. The data carrying sub-carriers are indexed by $k \in \{\pm 1, \cdots \pm \frac{N_c}{2}\}$. The discrete samples of the frequency domain

channel estimates obtained from the receiver are given by

$$\begin{aligned} h_1[k] &= \alpha_{\mathrm{d}_1} e^{-j2\pi f_c \tau_{\mathrm{d}_1}} e^{-j2\pi \frac{k}{N} \tau_{\mathrm{d}_1} f_s} + \alpha e^{-j2\pi f_c \tau} e^{-j2\pi \frac{k}{N} \tau f_s}, \\ h_2[k] &= \alpha_{\mathrm{d}_2} e^{-j2\pi f_c \tau_{\mathrm{d}_2}} e^{-j2\pi \frac{k}{N} \tau_{\mathrm{d}_2} f_s} + \alpha e^{-j(2\pi f_c \tau - \phi)} e^{-j2\pi \frac{k}{N} \tau f_s}. \end{aligned} \tag{2.3}$$

As mentioned in Chapter 1, there will be an additional delay $\Delta\tau_i$, $i \in \{1, 2\}$ introduced by the timing synchronization algorithm of the IEEE 802.11p receiver, the affect of which has not been explicitly shown in (2.3). This additional delay $\Delta\tau_i$ will be added to every delay in (2.3) thus changing the value of τ which is crucial for radar application. This timing offset does not affect the true purpose of DSRC, i.e., communication and is taken care of during channel equalization. This reiterates the point that the proposed algorithm makes use of the direct path as a timing reference and does not require access to the system clock. The frequency domain channel estimates are corrupted by samples of additive white Gaussian noise (AWGN) of variance σ^2.

2.2.1 Doppler model

If a target is moving with a relative velocity v_{rel} with respect to the radar, the reflected signal encounters a Doppler frequency shift f_{D} given by

$$f_{\mathrm{D}} = \frac{2v_{\mathrm{rel}}}{\lambda}. \tag{2.4}$$

Under the assumption that the signal bandwidth B is much smaller than the carrier frequency f_c (which is true for DSRC), the Doppler frequency shift f_{D} across the bandwidth can be approximated as constant. The Doppler frequency manifests itself as a continuous phase shift of $e^{j2\pi f_{\mathrm{D}} t}$ in the received

signal [7]. Due to small Doppler frequencies typically experienced in automotive settings, we use a first-order approximation with the Doppler phase assumed constant over the duration of one OFDM symbol [7]. The Doppler frequency results in a phase change of $2\pi f_{\mathrm{D}} T_{\mathrm{OFDM}}$ from one OFDM symbol to the next, where T_{OFDM} is the duration of one OFDM symbol. The modified discrete frequency domain channel estimates of the p^{th} OFDM symbol in a coherent processing interval (CPI) are given by

$$\begin{aligned} h_1[k] &= \alpha_{\mathrm{d}_1} e^{-j2\pi f_c \tau_{\mathrm{d}_1}} e^{-j2\pi \frac{k}{N} \tau_{\mathrm{d}_1} f_s} + \alpha e^{-j2\pi f_c \tau} e^{-j2\pi \frac{k}{N} \tau f_s} e^{-j2\pi p f_{\mathrm{D}} T_{\mathrm{OFDM}}}, \\ h_2[k] &= \alpha_{\mathrm{d}_2} e^{-j2\pi f_c \tau_{\mathrm{d}_2}} e^{-j2\pi \frac{k}{N} \tau_{\mathrm{d}_2} f_s} + \alpha e^{-j(2\pi f_c \tau - \phi)} e^{-j2\pi \frac{k}{N} \tau f_s} e^{-j2\pi p f_{\mathrm{D}} T_{\mathrm{OFDM}}}. \end{aligned} \tag{2.5}$$

2.3 Multi-target scenario

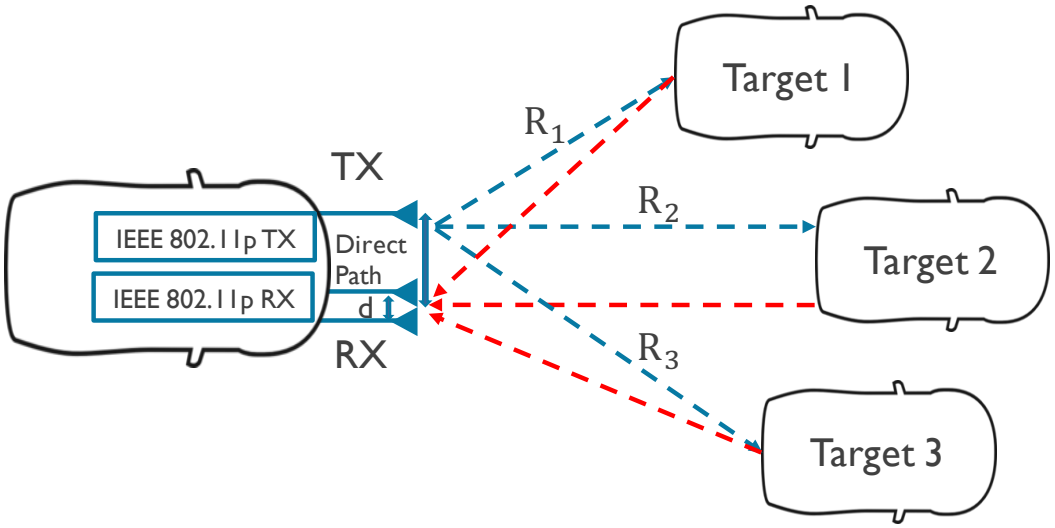

Figure 2.2: Multi-target channel model. This figure illustrate a multi-target radar scenario.

Fig. 2.2 shows a scenario with multiple targets. In case of multiple

targets, the radar will receive reflections from each target resulting in a summation over the second complex exponential in (2.3). Each reflected path will be parametrized with it's own set of parameters $[\alpha_\ell, \tau_\ell, \phi_\ell]$ dependent on the target distance, RCS and DoA. The resulting discrete frequency domain channel estimates assuming zero Doppler are given by

$$\begin{aligned} h_1[k] &= \alpha_{\mathrm{d}_1} e^{-j2\pi f_c \tau_{\mathrm{d}_1}} e^{-j2\pi \frac{k}{N} \tau_{\mathrm{d}_1} f_s} + \sum_{\ell=1}^{L} \alpha_\ell e^{-j2\pi f_c \tau_\ell} e^{-j2\pi \frac{k}{N} \tau_\ell f_s}, \\ h_2[k] &= \alpha_{\mathrm{d}_1} e^{-j2\pi f_c \tau_{\mathrm{d}_1}} e^{-j2\pi \frac{k}{N} \tau_{\mathrm{d}_1} f_s} + \sum_{\ell=1}^{L} \alpha_\ell e^{-j(2\pi f_c \tau_\ell - \phi_\ell)} e^{-j2\pi \frac{k}{N} \tau_\ell f_s}, \end{aligned} \tag{2.6}$$

where L denotes the total number of targets and ϕ_ℓ is related to the DoA θ_ℓ of the ℓ^{th} target by $\phi_\ell = \frac{2\pi \mathrm{d} \cos\theta_\ell}{\lambda}$.

2.4 DSRC signal model

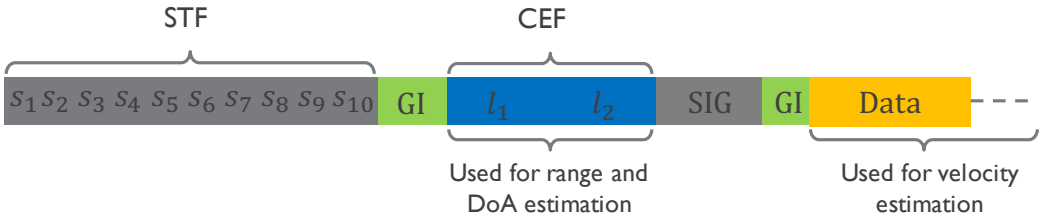

Figure 2.3: DSRC frame structure. The CEF is used for range and DoA estimation. Velocity is estimated using all the data symbols in the frame.

Fig. 2.3 illustrates an example of the IEEE 802.11p PHY frame structure used in DSRC. Each frame consists of a short training field (STF) consisting of ten short preambles, channel estimation field (CEF) consisting of two

long preambles, a signal field (SIG) followed by data symbols. In this work, a radar CPI corresponds to one DSRC frame in which during which the target parameters are assumed to remain fixed. We use the CEF for estimating the target range and DoA. The velocity estimation exploits all the data symbols in one DSRC frame.

Chapter 3

Range, DoA and velocity estimation algorithm

The formulation in Chapter 2 captures the parameters of interest, τ and ϕ as the frequency and phase of the two complex exponentials in (2.3). f_{D} is captured by the changing phase across multiple OFDM symbols as apparent in (2.5). In this chapter we first describe the LS-MP algorithm followed by the two step iterative LS-MP based range, DoA and velocity algorithms which operate on the sampled frequency domain channel estimates in (2.3) and (2.5). The algorithms are described from the perspective of one RX antenna, since multiple antennas are only required for DoA estimation.

3.1 LS-MP algorithm

LS-MP is a variant of the matching pursuit algorithm that iteratively tries to find a sparse representation of a signal vector using the least squares (LS) criterion at each iteration from a pre-defined over-complete dictionary. The LS-MP algorithm was originally proposed in [4] in the context of estimating rapidly varying sparse channels. In each successive iteration, the LS-MP algorithm selects a vector from the pre-defined dictionary which combined with the previously selected vectors gives the minimum squared residual error.

This procedure in general results in a more sparse representation of a signal [4]. The vector selected at the p^{th} iteration is

$$\mathbf{c_p} = \underset{\mathbf{c_j} \in \mathbf{C}, \mathbf{c_j} \notin \mathbf{C_{I_{p-1}}}}{\operatorname{argmin}} \|\mathbf{y} - \mathrm{LS}(\mathbf{y}, \mathbf{C_{I_{p-1}}}, \mathbf{c_j})\|^2, \tag{3.1}$$

where $\mathbf{C}$ denotes the pre-defined dictionary, $\mathbf{C_{I_{p-1}}}$ denotes the matrix formed by the vectors selected up to the p^{th} iteration, $\mathbf{y}$ is the signal whose sparse representation needs to be found and $\mathrm{LS}(\mathbf{y}, \mathbf{C_{I_{p-1}}}, \mathbf{c_j})$ represents the least squares solution of $\mathbf{y}$ in terms of the matrix $[\mathbf{C_{I_{p-1}}}, \mathbf{c_j}]$. This process is continued till a pre-specified stopping criterion is met.

3.2 LS-MP based range, DoA and velocity estimation

The sparse nature of the parameter space for our channel model in time domain makes LS-MP a suitable algorithm for our problem. The proposed algorithm operates on the frequency domain channel estimates which are in fact scaled and delayed complex exponentials corresponding to different delays as shown in (2.3). We use LS-MP to identify the sparse set of vectors which span the complex exponentials in (2.3) and their respective parameters which can then be mapped to range and DoA. The vectors forming the dictionary in this case are complex exponentials over a range of delays $\hat{\tau}_j \in \hat{\tau}_0, \hat{\tau}_1 \ldots \hat{\tau}_K$. We exploit the one-to-one mapping of target distance to the signal delay and define a distance grid $\mathcal{D} = \{\hat{d}_0, \hat{d}_1 \ldots \hat{d}_K\}$ in the range $[\hat{d}_0, \hat{d}_K]$, map these distance onto delays using $\hat{\tau}_j = \frac{2\hat{d}_j}{c}$ for $j \in 0, 1 \ldots K$ and then use these for forming the over-complete dictionary

$$\mathbf{C} = \begin{bmatrix} e^{-j2\pi \frac{0}{N_c} \hat{\tau}_0 f_s} & \dots & e^{-j2\pi \frac{0}{N_c} \hat{\tau}_K f_s} \\ \vdots & \ddots & \vdots \\ e^{-j2\pi \frac{N_c-1}{N_c} \hat{\tau}_0 f_s} & \dots & e^{-j2\pi \frac{N_c-1}{N_c} \hat{\tau}_K f_s} \end{bmatrix}. \tag{3.2}$$

The matrix $\mathbf{C}^{N_c \times K}$ consists of $K \in \mathbb{C}^{N_c}$ vectors corresponding to the elements of grid $\mathcal{D}$. The distance range $[\hat{d_0}, \hat{d_K}]$ can be determined from the signal transmit power and link budget analysis based on the path loss exponent and antenna gains. Unlike traditional radars, our setup does not have any integration gain and thus the range should be limited to the point where the signal starts falling below the noise floor to avoid unnecessary computation. In addition, the maximum unambiguous range is also limited by the duration of the cyclic prefix (CP) of the OFDM symbols.

3.2.1 Range estimation

The range estimation algorithm starts off by first estimating the delay of the direct path since it is much larger in magnitude. We observe that the direct path delay will not exactly be equal to one of the entries of the discretized distance grid $\mathcal{D}$. Any residual after the first iteration will still be much larger than the reflected signal. One solution to this problem is to increase the resolution of the distance grid $\mathcal{D}$. Doing this however increases the complexity that can be avoided by fine-tuning over a finer grid $\mathcal{D}'$ around the estimate $\hat{d}_{\max}$ obtained from $\mathcal{D}$. The point of maximum correlation $\hat{d}_{\max}$ will also be perturbed slightly due to the presence of the reflected signal. Under the parameters described in Chapter 5, the direct and reflected signals differ

in power anywhere from 40dB − 80dB depending on the range of the target. This drastic difference in power is the reason that we require very accurate estimate of the direct path parameters.

The issue of limited resolution of the grid $\mathcal{D}$ and presence of the reflected signal are tackled by jointly optimizing over the finer resolution grid $\mathcal{D}'$ for the direct path and the coarse grid $\mathcal{D}$ for the reflected path using the LS-MP algorithm for a joint solution $\hat{\mathbf{d}}_{\max}$. The delay $\hat{\tau}_{\mathrm{d}_\ell}$ corresponding to the chosen vector from the grid $\mathcal{D}'$ is our estimate of direct path delay τ_{d_i} and the corresponding correlation coefficient $c_{0\ell}$ is the estimate of the $\alpha_{\mathrm{d}_i} e^{-j2\pi f_c \tau_{\mathrm{d}_i}}$ parameter in (2.3) for $i, \ell = \{1, 2\}$. The delay corresponding to the second vector chosen from the grid $\mathcal{D}$, $\hat{\tau}$, is the estimate for τ in (2.3) which can then be mapped onto the target distance $\hat{R}$. The corresponding correlation coefficients, c_{11} and c_{12}, are the estimates of $\alpha e^{-j(2\pi f_c \tau)}$ and $\alpha e^{-j(2\pi f_c \tau - \phi)}$ in (2.3) for the first and second RX antenna.

An important point here is that jointly choosing first basis vector corresponding to the direct path and the second basis vector corresponding to the strongest target reflection minimizes the offset of the estimated direct path from the ground truth. Even though the strongest target signal is much (40dB −80dB) weaker than the direct signal, choosing the first basis vector only on the basis of maximum correlation results in a higher offset in the direct path estimation and consequently larger residues which affect the reflected path parameter estimation in an adverse manner.

For the multiple targets case, subsequent draws are made from the

coarse grid $\mathcal{D}$ until $|\hat{\mathbf{d}}_{\max}| = L + 1$, where L is the total number of targets if the number of targets is known or until the residual falls below the noise floor. In this work, we assume that the noise variance is known. In a practical setting, a noise variance estimator, such as [20],can be used. The estimated coefficients $c_{\ell 1}$ and $c_{\ell 2}$ and delay $\hat{\tau}_\ell$ correspond to the complex channel gain and delay of the ℓ^{th} target for $\ell \in 1 \dots L$.

3.2.2 DoA estimation

The DoA estimate does not require any additional computation and can be obtained from the parameters solved for earlier. The parameters for the direct paths of the two RX antennas, i.e. $\alpha_{\mathrm{d}_i}, \tau_{\mathrm{d}_i}$ for $i = \{1, 2\}$, are estimated independently since we require accurate estimates for these parameters as explained in Chapter 2. The parameters for the reflected signal, however, should be evaluated on the same grid $\mathcal{D}$ so as to not introduce any artificial bias in the estimates of $\alpha_\ell e^{-j(2\pi f_c \tau_\ell)}$ and $\alpha_\ell e^{-j(2\pi f_c \tau_\ell - \phi_\ell)}$ for $\ell \in 1 \dots L$. The DoA estimate $\hat{\theta}_\ell$ for the ℓ^{th} target is obtained by mapping back the phase difference $\Delta\Lambda_\ell = \angle c_{\ell 1}^* c_{\ell 2}$ using

$$\hat{\theta}_\ell = \cos^{-1}\left(\frac{\lambda \Delta\Lambda_\ell}{2\pi d}\right). \tag{3.3}$$

The LS-MP based range and DoA estimation procedure is summarized in Algorithm 1 for a single target scenario. Here LS() denotes the least squares solution as in (3.1).

Algorithm 1 LS-MP based range and DoA algorithm

procedure LS-MP($\mathbf{C}, \mathcal{D}, \mathbf{h}_i$)

$\hat{d}_{\max} = \underset{\mathbf{c}_k \in \mathbf{C}}{\operatorname{argmax}}\ \mathbf{h}_i^* \mathbf{c}_k$

Define $\mathcal{D}'$ around $\hat{d}_{\max}$ and $\mathbf{C}'$ using $\mathcal{D}'$ based on (3.2).

$\hat{\mathbf{d}}_{\max}, c_{11}, c_{12} = \underset{\substack{\mathbf{c}'_{k'} \in \mathbf{C}' \\ \mathbf{c}_k \in \mathbf{C}}}{\operatorname{argmin}} \left|\left| \mathbf{h}_i - \mathrm{LS}(\mathbf{h}_i, \mathbf{c}'_{k'}, \mathbf{c}_k) \right|\right|_2^2$

$[\hat{\tau}_{\mathrm{d}_i}, \hat{\tau}] \leftarrow \hat{\mathbf{d}}_{\max}$

$\hat{R} \leftarrow \hat{\tau}$

$\hat{\theta} \leftarrow \cos^{-1}\left(\frac{\lambda \Delta\Lambda}{2\pi d}\right), \Delta\Lambda = \angle c_{11}^* c_{12}$

3.2.3 Velocity estimation

The velocity/Doppler estimation algorithm is conceptually similar to successive interference cancellation in communication systems and uses the estimates from the range estimation stage. Doppler frequency offset due to relative motion of the target with respect to the radar exhibits itself as a varying phase from one OFDM symbol to the next modeled in (2.5).

The direct path is cancelled by the signal reconstructed using the parameters $[c_{01}, c_{02}, \hat{\tau}_{\mathrm{d}_1}, \hat{\tau}_{\mathrm{d}_2}]$ estimated by the range algorithm. After direct path cancellation, the radar RX decodes the OFDM data symbols received through the path reflected from the target. The RX makes use of the N_p pilot subcarriers embedded in each OFDM symbol to keep track of the changing phase from each OFDM symbol to the next. Linear least squares regression is used to estimate the doppler frequency $\hat{f}_{\mathrm{D}}$. The estimated velocity $\hat{v}_{\mathrm{rel}}$ is obtained

from $\hat{f}_{\mathrm{D}}$ using

$$\hat{v}_{\mathrm{rel}} = \frac{\hat{f}_{\mathrm{D}}\lambda}{2}. \tag{3.4}$$

We note here that velocity estimation requires observation of a larger number of OFDM symbols for good estimation performance. In radar literature, this is called the *dwell time* [21]. Larger dwell times lead to better estimation performance in terms of mean squared sense and resolution. Another point worth noting is that, the maximum unambiguous velocity estimation range is determined by T_{OFDM}, the time duration of one OFDM symbol. Assuming the same number of total sub-carriers, an OFDM signal with twice the bandwidth would have twice the maximum unambiguous range.

In case of a multi-target scenario, the signal corresponding to the ℓ^{th} strongest reflector is cancelled by it's reconstructed copy obtained using the parameters $[c_{\ell 1}, c_{\ell 2}, \hat{\tau}_{\ell}]$ estimated by the range algorithm. The decoding process is continued until the residue signal falls below the noise threshold.

Fig. 3.1 illustrates the complete range, DoA and velocity estimation algorithm procedure. Stage 1 on the left estimates the range and DoA using Algorithm 1. Stage 2 depicted on the right uses the estimates from stage 1 and successive signal cancellation to form the velocity estimate.

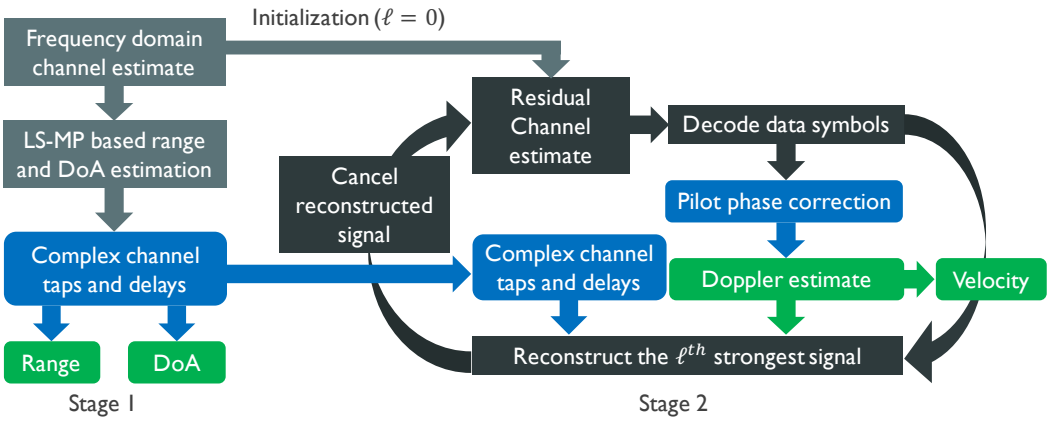

Figure 3.1: Range, DoA and velocity estimation algorithm. Stage 1 uses LS-MP to form range and DoA estimates. Stage 2 uses the estimates from stage 1 and successive signal cancellation for velocity estimation.

Chapter 4

Cramer-Rao lower bound

This Chapter provides a *very* brief overview of the CRLB. CRLB is a lower bound on the variance of any unbiased estimator and serves as a theoretical performance benchmark. It is the minimum variance that an unbiased estimator of the parameter of interest can attain. The CRLB is calculated using the inverse of the fisher information matrix (FIM). FIM is a measure of the amount of information that a signal observation conveys about a particular parameter. Under AWGN corrupted observations of a signal $y[n] = x[n; \mathbf{\Theta}]+w[n]$ for $n \in 1 \dots N$, the FIM is given by [21]

$$\mathbf{I}(\mathbf{\Theta}) = \frac{1}{\sigma^2} \sum_{n=1}^{N} \left(\frac{\partial x[n; \mathbf{\Theta}]}{\partial \mathbf{\Theta}} \right)^2 , \tag{4.1}$$

where σ^2 is the variance of the noise $w[n]$ and $\mathbf{\Theta}$ is the parameter vector of interest.We refer the interested reader to [21] for a more detailed overview on CRLB for various radar parameters of interest. The details of the CRLB computation for the results herein are out of the scope of this report and are not provided. In the following, we give some interesting CRLB results that will be useful for comparison in Chapter 5.

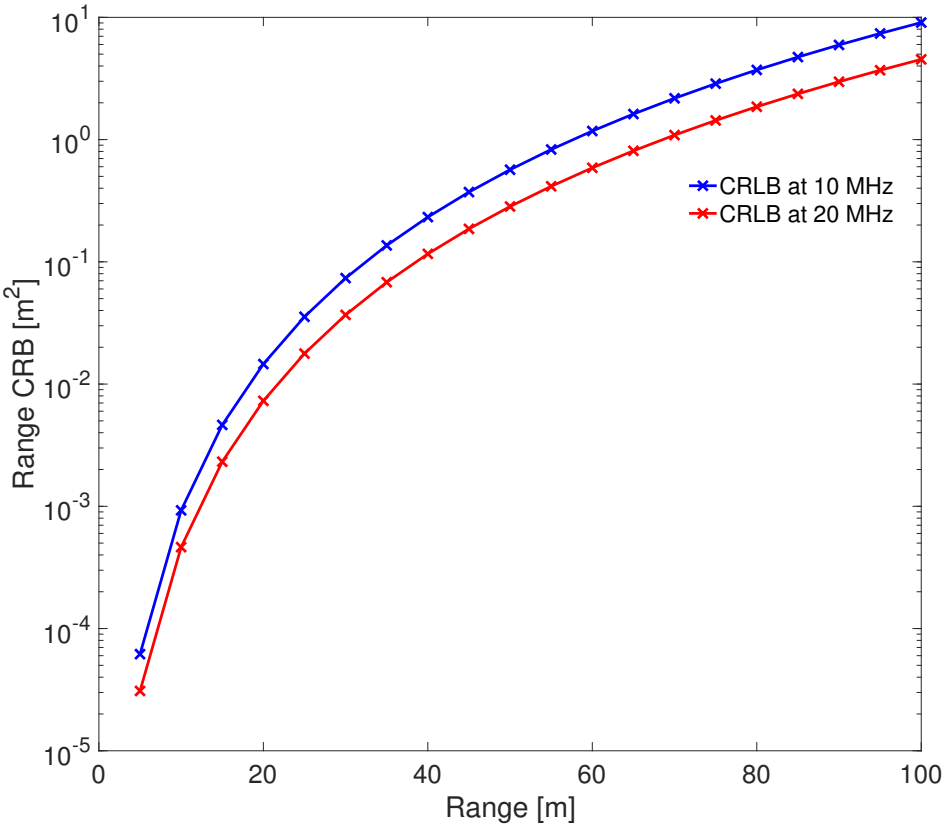

Figure 4.1: Range CRLB for an OFDM waveform of bandwidths 10 MHz and 20 MHz.

4.1 Effect of bandwidth on CRLB

Fig. 4.1 illustrates the CRLB for the range parameter for a OFDM waveform in a single target setting without including direct signal interference (DSI) into the model. The results show that performance improves by a factor of two for a two-fold increase in the waveform bandwidth. This is because the CRLB for range is inversely proportional to the squared of bandwidth. This more than offsets the increased noise due to the higher bandwidth.

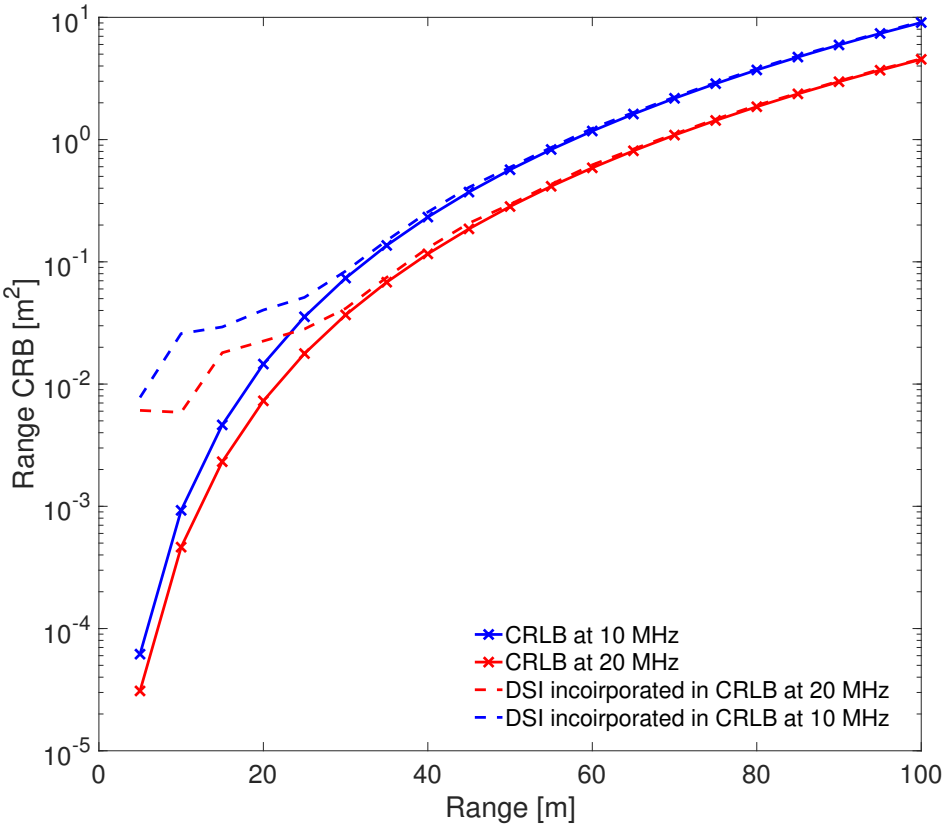

Figure 4.2: Effect of including DSI on range CRLB for an OFDM waveform.

4.2 Effect of direct signal interference on CRLB

Fig. 4.2 is obtained under the same settings as Fig. 4.1 with the modification of including the string DSI into the channel model. As is clear from the results, the CRLB deteriorates for targets close to the radar. This is because the direct signal and the reflected signal are separated by less than the achievable resolution of the radar given by $\frac{c}{2B}$, where c is the speed of light and B is the waveform bandwidth. As we will see in Chapter 5, the proposed

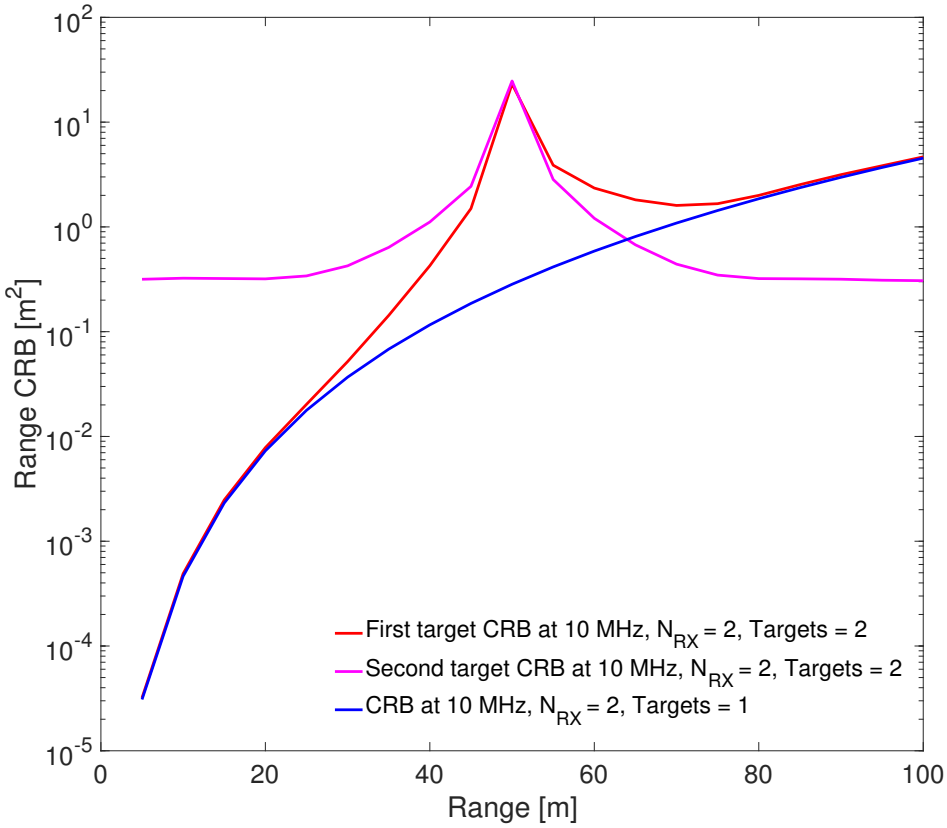

Figure 4.3: Comparison of range CRLB for a single target scenario and a two target scenario. Fig. illustrates that as the two targets get close to one another, they can not be separated.

algorithm's performance also suffers in this region.

4.3 Effect of multiple targets on CRLB

Fig. 4.3 plots the range CRLB for a two-target scenario. The solid blue line (—) is the reference CRLB for a single target. For the two-target setting, the solid magenta line (—) plots the CRLB of the target held fixed at 50m.

The other target is moved from 10m to 100m with it's CRLB shown by the solid red line (—). As the two targets start getting close to each other (closer than the resolution limit), the CRLB starts to blow up. This makes intuitive sense in that as the targets get closer and closer, we can not separate them visually. The CRLB for the moving target returns to the value of the single target CRLB after adequate separation between the two targets.

Chapter 5

Results and discussion

This Chapter describes the simulation setup and parameters used to evaluate the performance of the algorithms, presents results and includes a brief discussion on the results.

5.1 Simulation setup

Our simulation setup consists of a IEEE 802.11p type PHY implemented in MATLAB. The receiver provides the frequency domain least squares based channel estimates using the CEF of IEEE 802.11p shown in Fig. 2.3. The antenna placement follows the setup shown in Fig. 2.1 with the TX antenna separated from the RX antennas by 1.5m. We assume omnidirectional antennas with a 5dBi gain. The important parameters of the PHY layer are summarized in Table 5.1.

The frequency offset is assumed be the zero because the local oscillator is shared by all the RF chains. The timing synchronization algorithm is modeled as a uniform random variable introduced as a delay in the received signal. We evaluate the performance of the algorithm over a 2-D grid with targets distributed uniformly in range and angle. The target range R is varied

Bandwidth B	10 , 20 MHz
Sampling frequency f_s	10 , 20 MHz
Carrier frequency f_c	5.89 GHz
Number of data sub-carriers N_c	52
Transmit power	20 dBm
Antenna gain	5 dBi
Path loss coefficient	2
Target cross-section coefficient ζ	1
Power in Rayleigh path as percentage of LOS path power γ	0 , 2 , 10 %
ADC quantization level	∞ , 14 , 12 bits

Table 5.1: IEEE 802.11p PHY and simulation parameters

from 5m to 60m and the angles θ is varied from 20° to 160°. One important thing to point here is that the maximum detection range of the IEEE 802.11p radar is limited by the cyclic prefix length of the OFDM symbols. Any delay in excess of that will result in inter-symbol interference. Our simulations are limited to an even smaller range of 60m because the signal starts falling below the noise floor after this range.

5.2 Results - LS-MP

5.2.1 Sterling type 0 targets

Fig. 5.1 shows the root mean square error (RMSE) of the target range estimate for different values of B and the corresponding CRLB as a function of the true target range R [21]. Fig. 5.1 also plots the RMSE in range estimate assuming perfect cancellation of the direct path. The CRLB plotted in Fig. 5.1 assumes perfect cancellation of the direct path [21] and is the same as

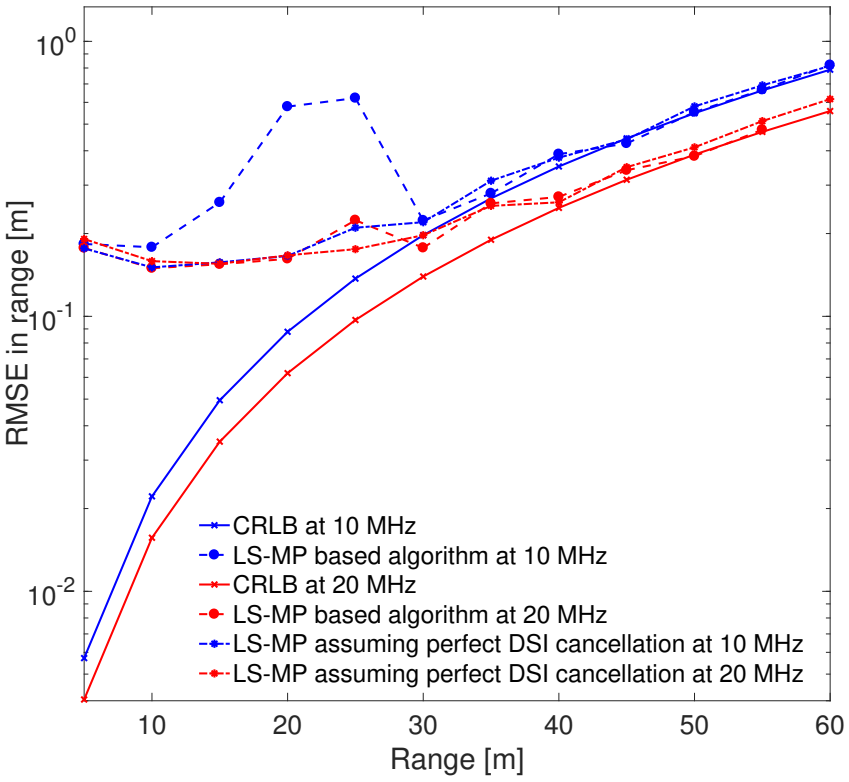

Figure 5.1: RMSE of the range estimate using the LS-MP algorithm and the CRLB for $B = 10$MHz and $B = 20$MHz.

shown in Fig. 4.1. It can be observed that the algorithm performs better for a larger system bandwidth. The reason for improved performance at 20 MHz is the larger separation of the dictionary vectors in the frequency domain for the same target distances. The initial bump in the RMSE results of Fig. 5.1 is explained by the fact that the algorithm does not achieve the CRLB for smaller distances because the frequency separation of the two sinusoids is much smaller

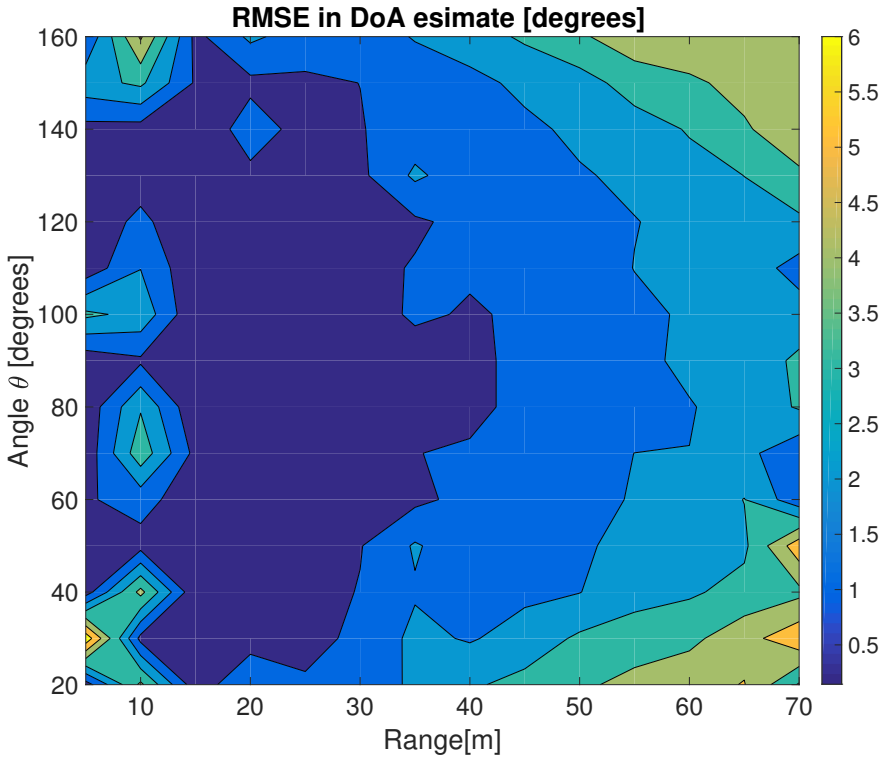

Figure 5.2: RMSE of the DoA estimate using LS-MP algorithm at 10 MHz. The RMSE stays under 2° for targets up to 55m away.

than the Rayleigh limit. The two sinusoids being close together in frequency make the estimation of the parameters of the direct path erroneous, hence contributing to errors in the estimation of parameters of the reflected path in the second step of the algorithm. For larger distances, the frequency separation is large enough to achieve the CRLB. Fig. 5.1 also shows an error floor for the case of perfect cancellation of the direct path. This can be attributed to the fact that LS-MP picks the best vector from the pre-defined dictionary

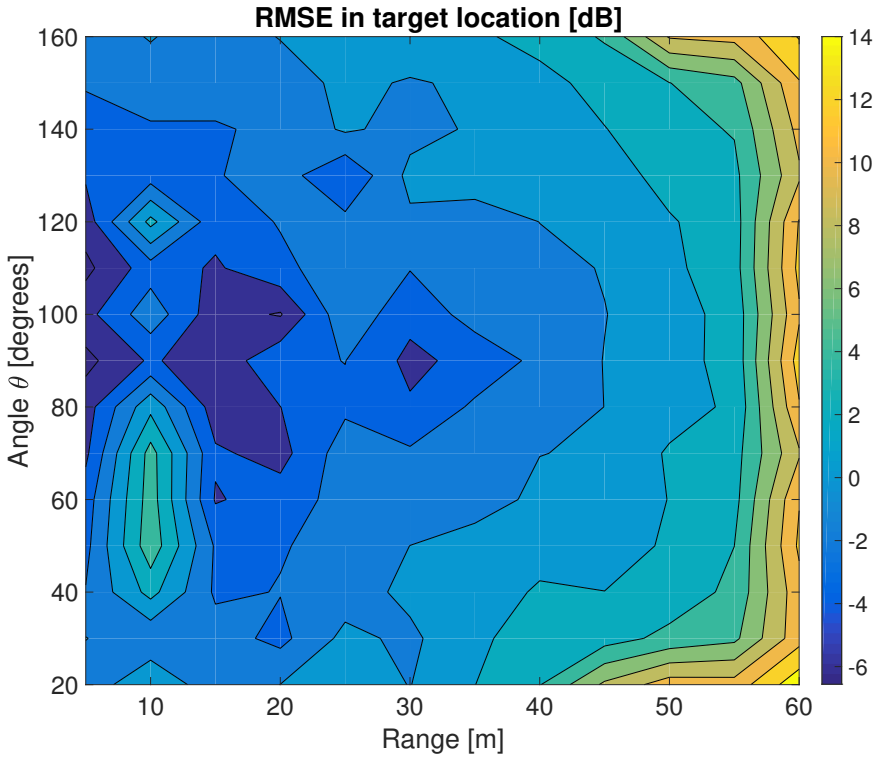

Figure 5.3: RMSE of the target location using the LS-MP algorithm in dB scale at 10 MHz. 0 dB corresponds to an error of 1m in target location.

and thus has a strong dependance on the resolution of the distance grid $\mathcal{D}$ described in Section 3.2. The distance grid $\mathcal{D}$ used to compute these results had a resolution of 1m. Finally it can be seen that the range error is under 1m for distances up to 60m.

Fig. 5.2 shows the RMSE in the target DoA estimate. The DoA RMSE is well under 2° for a large portion of the grid. As expected for any DoA algorithm, the performance deteriorates for angles near to the end-fire direction.

Fig. 5.3 combines the error in the DoA estimate with the range estimate error to represent the error in the position of the estimated targets from their true location. The error in target location is under 1m for targets up to a range of 45m.

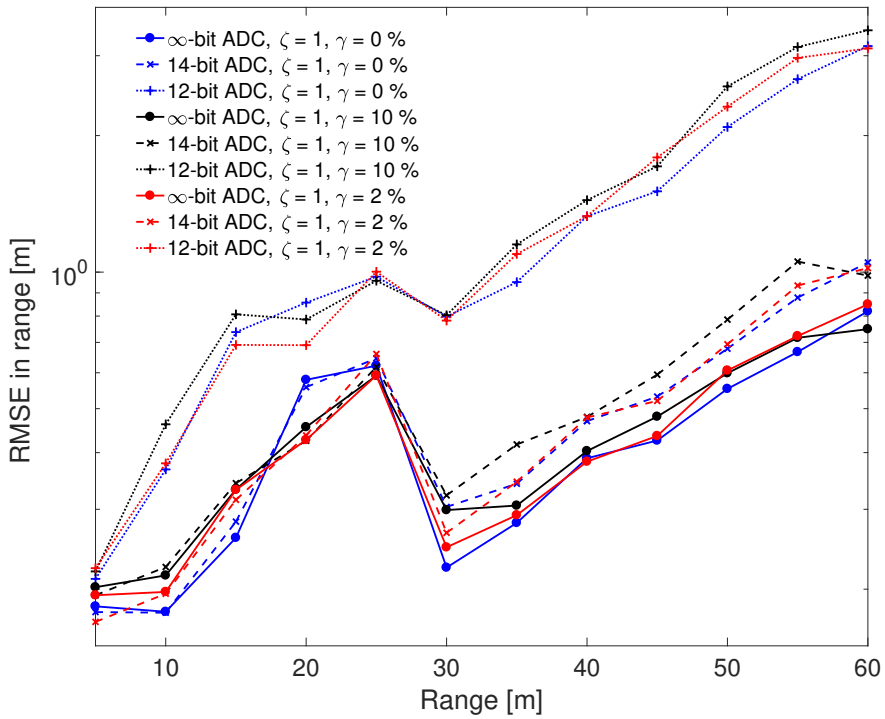

Figure 5.4: RMSE of the range estimate using the LS-MP algorithm for different values of rayleigh power parameter γ and ADC quantization levels. As shown, the RMSE gets worse with increasing γ and lower ADC resolution.

5.2.2 Sterling type 3 targets

Fig. 5.4 compares the performance of Sterling type 3 targets for different values of the parameter γ with fixed RCS area Swerling type 1 targets. It can be seen in each of the three sets of quantization curves that a larger value of the γ parameter corresponds to a higher RMSE. The different paths of the Rayleigh part of the received signal, which correspond to a high scattering environment around the target, can not be distinguished from one another to use in a constructive manner and interfere with the LOS signal. This is similar to fading effects in communication channels. The DoA estimate is similarly adversely affected by increasing γ values.

5.2.3 Quantization effects

Fig. 5.4 also shows the RMSE in target range estimate for different levels of analog-to-digital (ADC) quantization. As can be seen, the RMSE performance get progressively worse with lower ADC resolution levels. The direct signal interference in our setup is $40\text{dB} - 80\text{dB}$ stronger than the signal of interest depending on the target range. This huge power difference consumes a major part of the ADC dynamic range, thus inducing a very coarse quantization of the signal of interest. According to the 6dB rule of thumb, even in the case of strongest of the targets the first 7 bits are consumed by the direct signal interference. Commercial radars commonly use $12-14$ bit ADCs. WiFi and DSRC chips available in the market commonly employ $6-8$ bit ADCs and thus for our joint radar-communication solution to work effectively a higher

resolution ADC is required.

5.2.4 Velocity results

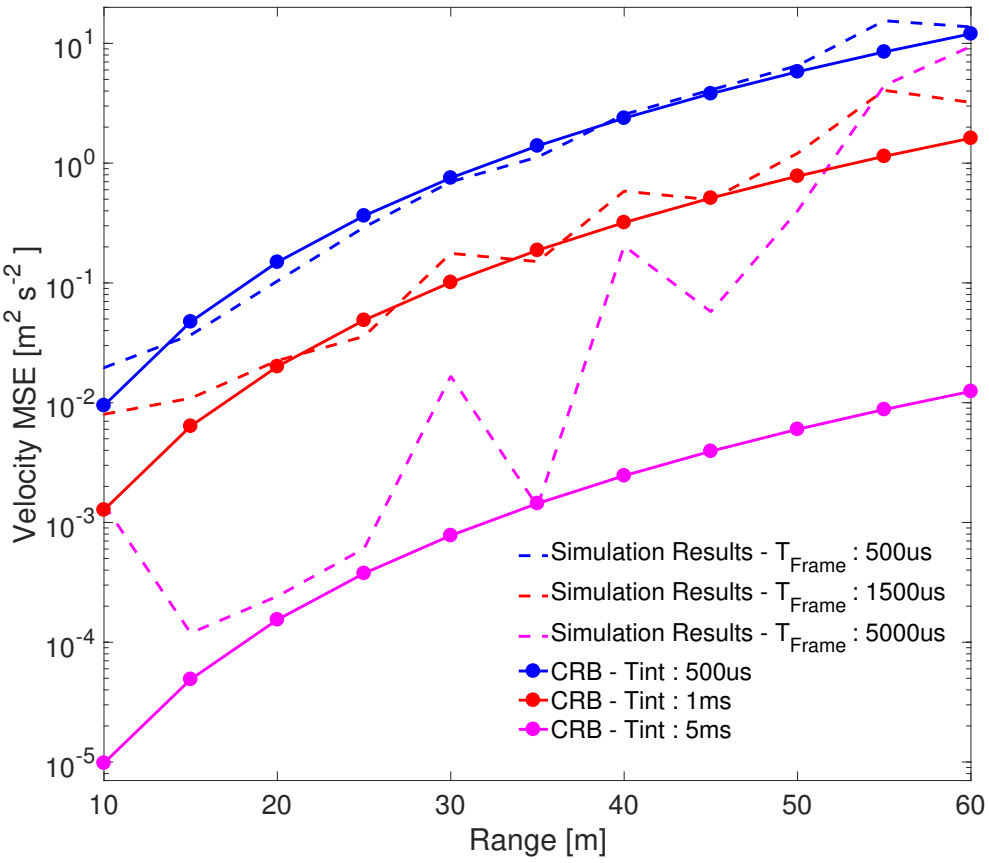

Figure 5.5: MSE of the velocity estimation using the successive signal cancellation algorithm for different values of T_{Frame}. CRLB of the velocity estimate is also plotted alongside.

Fig. 5.5 shows the performance of the successive signal cancellation based velocity estimation algorithm for a target located at broadside. The CRLB of the velocity estimate is also plotted alongside for performance com-

parison [22]. T_{Frame} is the length of one DSRC frame. A typical DSRC frame is $\approx 500\mu$s. As can be seen, the performance improves with an increasing dwell time as expected. Due to the interference cancellation nature of the algorithm, estimation errors from previous stages are propagated to the next stages and have an adverse effect on the estimation performance.

5.2.5 Multiple targets

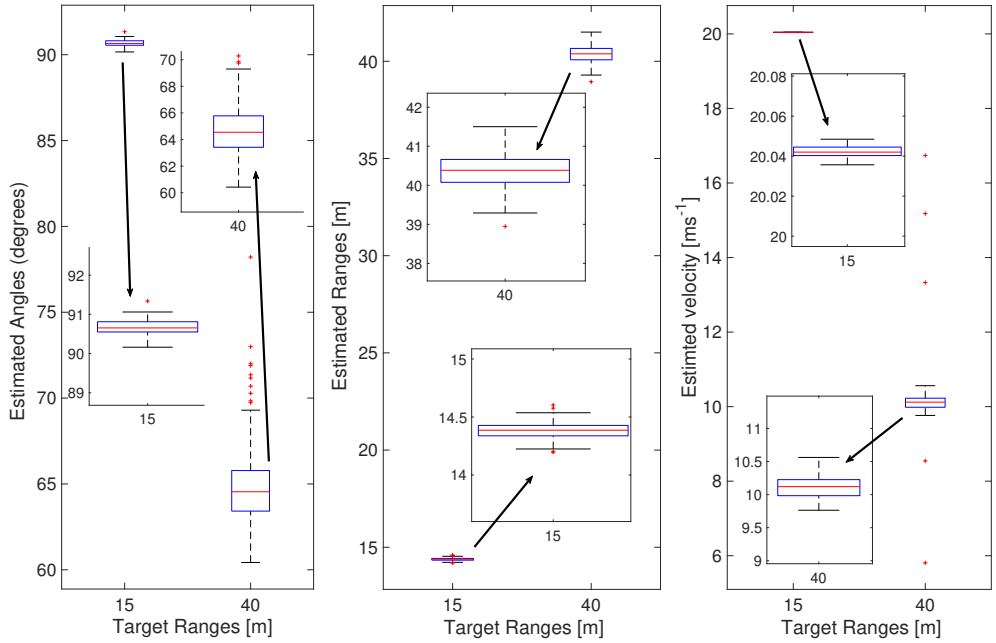

Figure 5.6: Demo run of the proposed algorithm on a two target scenario.

Fig. 5.6 demonstrates the application of the proposed solution on one representative two-target setting. The first target is at 15m at an angle of 90° and has a relative velocity of 20m/s. The second target is at 40m at an angle of 40° and has a relative velocity of 10m/s. The estimated parameters over 100

runs of the above setting are presented using the boxplot of each parameter vs the true targets range. Results show that, other than a few iterations of the velocity estimate of second target, the median of each box is very close to it's respective ground truth value and the interquartile range is matches the singe target results shown earlier.

5.2.6 Comparison with FMCW

RMSE results for a frequency modulated continuous-waveform (FMCW) radar are reported in [23] for a bandwidth of 100 MHz for a 4-element uniform linear array (ULA). At a signal-to-noise (SNR) ratio of 10dB per antenna element they report a RMSE of 0.015m in a single target scenario. Our algorithm at 10dB achieves a RMSE of 0.2m with a bandwidth of only 10MHz. The CRLB of the range estimate is inversely proportional to the square of bandwidth and the number of antenna elements. Taking into account the greater bandwidth (10x) and larger number of antennas (2x), our algorithm achieves comparable performance while being adversely affected by the guard bands of the OFDM signal waveform and the presence of the strong direct path which are absent in the setup considered in [23].

Chapter 6

Conclusion

This report presented a framework for an IEEE 802.11p based radar that operates on the frequency domain channel estimates generated by the DSRC PHY. It is a cost-effective joint radar-communication solution and can easily be integrated with DSRC. The channel model considered incorporates self-interference because of the mono-static nature of the radar setup and omnidirectional gain of antennas designed for communication. The results presented show a sub-meter RMSE in range estimation for targets up to distances of 60m. The DoA RMSE also stays under 2° for a large portion of the 2-D grid. A velocity estimation algorithm based on successive signal cancellation was also proposed. The results achieved the CRLB at medium to larger target distances, failing to do so at smaller ranges due to the strong direct signal interference and limited resolution because of the small DSRC bandwidth. The detailed numerical evaluation carried out in this report allows us to conclude that, the DSRC setup despite being severely constrained in terms of the signal bandwidth, number of antennas and antenna directivity pattern, can still achieve sub-meter accuracy in a sparse setting, for example a highway. Future work in this will explore using multiple DSRC frames to increase the dwell time for velocity estimation and tracking the phase inside an OFDM symbol.

Bibliography

[1] NTSB, "The use of forward collision avoidance systems to prevent and mitigate rear-end crashes," National Transportation Safety Board, Special Investigation Report, 2015.

[2] J. Hasch, E. Topak, R. Schnabel, T. Zwick, R. Weigel, and C. Waldschmidt, "Millimeter-wave technology for automotive radar sensors in the 77 ghz frequency band," *IEEE Transactions on Microwave Theory and Techniques*, vol. 60, no. 3, pp. 845–860, March 2012.

[3] J. B. Kenney, "Dedicated short-range communications (DSRC) standards in the united states," *Proc. of the IEEE*, vol. 99, no. 7, pp. 1162–1182, July 2011.

[4] W. Li and J. C. Preisig, "Estimation of rapidly time-varying sparse channels," *IEEE Journal of Oceanic Engineering*, vol. 32, no. 4, pp. 927–939, Oct 2007.

[5] C. Sturm, E. Pancera, T. Zwick, and W. Wiesbeck, "A novel approach to OFDM radar processing," in *Proc. of IEEE Radar Conference*, May 2009, pp. 1–4.

[6] G. Kalverkamp, B. Schaffer, and E. Biebl, "OFDM-based ranging approach for vehicular safety applications," in *Proc. of 2013 IEEE 78th*

Vehicular Technology Conference (VTC Fall), Sept 2013, pp. 1–5.

[7] L. Reichardt, C. Sturm, F. Grunhaupt, and T. Zwick, "Demonstrating the use of the IEEE 802.11p car-to-car communication standard for automotive radar," in *Proc. of 6th European Conference on Antennas and Propagation (EUCAP)*, March 2012, pp. 1576–1580.

[8] L. Dai, Z. Wang, J. Wang, and Z. Yang, "Positioning with OFDM signals for the next- generation GNSS," *IEEE Transactions on Consumer Electronics*, vol. 56, no. 2, pp. 374–379, May 2010.

[9] X. Li and K. Pahlavan, "Super-resolution TOA estimation with diversity for indoor geolocation," *IEEE Transactions on Wireless Communications*, vol. 3, no. 1, pp. 224–234, Jan 2004.

[10] F. Colone, P. Falcone, C. Bongioanni, and P. Lombardo, "WiFi-based passive bistatic radar: Data processing schemes and experimental results," *IEEE Transactions on Aerospace and Electronic Systems*, vol. 48, no. 2, pp. 1061–1079, APRIL 2012.

[11] R. C. Daniels, E. R. Yeh, and R. W. Heath, "Cost-effective vehicular radar through minimally-modified IEEE 802.11 devices," in *Radar Conference (RadarConf), 2017 IEEE.* IEEE, 2017, pp. 0675–0680.

[12] R. C. Daniels, E. R. Yeh, and R. W. Heath, "Forward collision vehicular radar with IEEE 802.11: Feasibility demonstration through measure-

ments," *IEEE Transactions on Vehicular Technology*, vol. 67, no. 2, pp. 1404–1416, Feb 2018.

[13] A. Sabharwal, P. Schniter, D. Guo, D. W. Bliss, S. Rangarajan, and R. Wichman, "In-band full-duplex wireless: Challenges and opportunities," *IEEE Journal on Selected Areas in Communications*, vol. 32, no. 9, pp. 1637–1652, Sept 2014.

[14] F. Colone, D. W. O'Hagan, P. Lombardo, and C. J. Baker, "A multistage processing algorithm for disturbance removal and target detection in passive bistatic radar," *IEEE Transactions on Aerospace and Electronic Systems*, vol. 45, no. 2, pp. 698–722, April 2009.

[15] R. Cardinali, F. Colone, C. Ferretti, and P. Lombardo, "Comparison of clutter and multipath cancellation techniques for passive radar," in *Proc. of IEEE Radar Conference*, April 2007, pp. 469–474.

[16] A. Lin and H. Ling, "Doppler and direction-of-arrival (DDOA) radar for multiple-mover sensing," *IEEE Transactions on Aerospace and Electronic Systems*, vol. 43, no. 4, pp. 1496–1509, October 2007.

[17] S. A. Zekavat, A. Kolbus, X. Yang, Z. Wang, J. Pourrostam, and M. Pourkhaatoun, "A novel implementation of DOA estimation for node localization on software defined radios: Achieving high performance with low complexity," in *Proc. of IEEE International Conference on Signal Processing and Communications*, Nov 2007, pp. 983–986.

[18] K. Usman Mazher, T. Shimizu, R. W. Heath, and G. Bansal, "Automotive radar using IEEE 802.11p signals," in *Proc. of 2018 IEEE Wireless Communications and Networking Conference (WCNC)*, April 2018, pp. 1–6.

[19] W. D. Blair and M. B. Pearce, "Monopulse processing for tracking unresolved targets," Naval Surface Warfare Center Dahlgren Div VA, Tech. Rep., 1997.

[20] T. Cui and C. Tellambura, "Power delay profile and noise variance estimation for OFDM," *IEEE Communications Letters*, vol. 10, no. 1, pp. 25–27, Jan 2006.

[21] M. A. Richards, *Fundamentals of radar signal processing.* Tata McGraw-Hill Education, 2005.

[22] P. Kumari, J. Choi, N. Gonzlez-Prelcic, and R. W. Heath, "IEEE 802.11ad-based radar: An approach to joint vehicular communication-radar system," *IEEE Transactions on Vehicular Technology*, vol. 67, no. 4, pp. 3012–3027, April 2018.

[23] D. Oh and J.-H. Lee, "Low-complexity range-azimuth FMCW radar sensor using joint angle and delay estimation without SVD and EVD," *IEEE Sensors Journal*, vol. 15, no. 9, pp. 4799–4811, 2015.

Vita

Khurram is a graduate student in the ECE department at the University of Texas at Austin. He finished his undergraduate studies from Lahore University of Management Sciences, Pakistan in May 2015. His academic interests lie in the area of signal processing applications in radar, communication and navigation. His "non-academic" interests include hiking, football, driving, traveling and reading amongst numerous others.

Permanent address: khurram.usman@utexas.edu

This report was typeset with LaTeX[†] by the author.

[†]LaTeX is a document preparation system developed by Leslie Lamport as a special version of Donald Knuth's TeX Program.